Ab initio investigation of the elasticity and stability of aluminium

Ab initio investigation of the elasticity and stability of aluminium

Weixue Li and Tzuchiang Wang

LNM, Institute of Mechanics, Chinese Academy of Science, Beijing, 100080, People's Republic of China

Abstract. On the basis of the pseudopotential plane-wave (PP-PW) method in combination with the local density functional theory (LDFT), complete stress–strain curves for the uniaxial loading and uniaxial deformation along the [001] and [111] directions, and the biaxial proportional extension along [010] and [001] for aluminium are obtained. During the uniaxial loading, certain general behaviours of the energy versus the stretch and the load versus the stretch are confirmed; in each case, there exist three special unstressed structures: f.c.c., b.c.c., and f.c.t. for [001]; f.c.c., s.c., and b.c.c. for [111]. Using stability criteria, we find that all of these states are unstable, and always occur together with shear instability, except the natural f.c.c. structure. A Bain transformation from the stable f.c.c. structure to the stable b.c.c. configuration cannot be obtained by uniaxial compression along any equivalent [001] and [111] direction. The tensile strengths are similar for the two directions. For the higher energy barrier of the [111] direction, the compressive strength is greater than that for the [001] direction. With increase in the ratio of the biaxial proportional extension, the stress and tensile strength increase; however, the critical strain does not change significantly. Our results add to the existing *ab initio* database for use in fitting and testing interatomic potentials.

1. Introduction

Investigation of the elastic behaviour of a perfect single crystal under loading is of interest. It can, for example, be carried out on a system in which substantial, elastic (but not necessary linear) deformation may occur, in which case substantial deformation may occur either without significant dislocation movement or before the deformation caused by dislocation movement becomes dominant. Deformation of whiskers, twinning, and martensitic transformations are relevant examples. The instability and branching under loading is related to the ideal strength and transformation. Such information is very useful in the analysis of the structural response in solids, e.g. polymorphism, amorphization, and melting to fracture.

Although Born [1] criteria are widely used in the investigation of strength, they are only valid under zero load. On the basis of a series of comprehensive theoretical and computational studies, Hill and Milstein [2–7] pointed out the following:

(i) stability is relative and coordinate dependent; and
(ii) different choices of the strain measure lead to different domains of stability.

On the basis of the Morse potential, they investigated the mechanical response of perfect crystal, including the stress–strain relation, instability, branching, and the strength of f.c.c.

Cu [8], f.c.c. Ni [10–12], and α-Fe [9], for different loading modes (e.g. uniaxial loading, uniaxial deformation, and shear loading; here, 'uniaxial loading' means that uniaxial stress is applied to one axis, and the lateral face is relaxed and stress-free (traction-free), while 'uniaxial deformation' just means that one axis is dilated or contracted, and the dimensions of the other two axes are fixed; in uniaxial deformation, all three axes are subjected to loading). The loading directions which were adopted included [001], [110], and [111]. Possible branching paths were revealed. Using the thermodynamic Gibb function, Wang *et al* [13, 14] developed an equivalent-stability analysis method, and investigated the onset of instability in a homogeneous lattice under critical loading. The onset modes, derived from the stability criteria, were verified by means of a molecular dynamics simulation. Zhou and Joós [15] derived general expressions for the stability criteria by an appropriate thermodynamic potential.

There has been less investigation based on first principles. Senoo *et al* [16] discussed the elastic deformation due to [100] loading of Al, using the pseudopotential method. Esposito *et al* [17] dealt with the tensile strength of f.c.c. Cu under uniaxial deformation on the basis of the *ab initio* potential, augmented-spherical-wave (ASW), and KKR methods. However, relaxation of the crystal structure was not permitted. Paxton *et al* [18] calculated the theoretical strength of five b.c.c. transition metals, and Ir, Cu, and Al, by considering ideal-twin stresses using the full-potential linear muffin-tin orbital (FP-LMTO) technique. Šob *et al* [19] investigated the theoretical tensile stress in tungsten single crystal under [001] and [111] loading by the FP-LMTO method. The stability analysis was not explicit in any of the above cases.

Bain transformation takes a crystal from its stable b.c.c. configuration into a stable f.c.c. structure, and vice versa, by means of homogeneous axial deformations. Which path requires the lowest energy and stress barrier between these states was investigated and reviewed by Milstein *et al* [20]. The general mechanics and energetics of the Bain transformation were presented. On the basis of the empirical pseudopotential, Milstein *et al* [20] investigated the Bain transformation of crystalline sodium in detail. This kind of transformation is also relevant to the investigation of epitaxial thin film [21].

In this paper, we present a direct investigation of the elasticity, the stress–strain relation, the stability, and the ideal strength of f.c.c. aluminium within density functional theory. The stability analysis is considered explicitly, on the basis of the theory of Hill, Milstein [2, 3, 7] and Wang *et al* [13, 14]. We consider several loading modes: uniaxial deformation and uniaxial loading along the [001] and [111] directions, and biaxial proportional extension along [001] and [010]. The deformation is homogeneous, elastic, and permitted to be appropriately large. The stress–strain relations are calculated, and the ideal strength is approached via the loss of stability. Branching or structural transformation from a primary path of deformation takes place with the loss or exchange of stability, which are relevant to the Bain transformation. In this way, the mechanical responses for different loading modes and directions are obtained clearly, from first principles.

The paper is organized as follows. The calculation model is presented in section 2. In this section, we give the formulation of the stress, elastic stiffness coefficients, and stability criteria, especially for three loading modes. The numerical precision is evaluated at the end of this section. As a benchmark, equilibrium properties and elastic constants are calculated in section 3, [001] uniaxial deformation and [001] uniaxial loading are considered in section 4, and a stability analysis is implemented. In section 5, [111] uniaxial deformation and [111] uniaxial loading are considered. Results on the biaxial proportional extension are given in section 6. *Ab initio* calculations can be used to construct a database for fitting and testing interatomic potentials [22, 23]; a brief discussion of our results together with the existing

ab initio database for aluminium is given in section 7. A summary and conclusions are presented in the last section.

2. Formulation

Consider an initial unstressed and unstrained configuration, denoted as $\mathbf{X_0}$. It undergoes homogeneous deformation under a uniform applied load, and changes from $\mathbf{X_0}$ to $\mathbf{X} = \mathbf{JX_0}$, where $\mathbf{J}$ is the deformation gradient or the Jacobian matrix and the rotation part is subtracted. The associated Lagrangian strain tensor $\mathbf{E}$ is

$$\mathbf{E} = \frac{1}{2}(\mathbf{J}^{\mathrm{T}}\mathbf{J} - \mathbf{I}) \tag{1}$$

and the physical strain is

$$\mathbf{e} = (\mathbf{J}^{\mathrm{T}}\mathbf{J})^{1/2} - \mathbf{I}. \tag{2}$$

For the present deformation, the internal energy U is rotationally invariant, and therefore only a function of $\mathbf{E}$. The second Piloa–Kirchhoff stress tensor $\mathbf{T}$ [24] is defined as

$$T_{ij} = \frac{1}{V_0} \frac{\partial U}{\partial E_{ij}}. \tag{3}$$

It relates the Cauchy stress, i.e., the true stress τ_{kl}, by the following equation:

$$T_{ij} = \det |\mathbf{J}| J_{ik}^{-1} J_{jl}^{-1} \tau_{kl} \tag{4}$$

where $\det |\mathbf{J}|$ is the ratio V/V_0. From the Cauchy stress, the applied force can be obtained by multiplying by the current transverse area.

For the stressed state $\mathbf{X}$, the elastic constants are determined through the equation

$$C_{ijkl}(\mathbf{X}) = \frac{1}{V(\mathbf{X})} \left(\frac{\partial^2 U}{\partial E'_{ij} \partial E'_{kl}} \Big|_{E'=0} \right) \tag{5}$$

where $\mathbf{E}'$ is the Lagrangian strain around the state $\mathbf{X}$. These elastic constants are symmetric with respect to interchange of indices, and are often expressed in condensed Voigt notation.

To analyse the stability, the elastic stiffness coefficient $\mathbf{B}$ [14] is introduced as follows:

$$B_{ijkl} = C_{ijkl} + \frac{1}{2}(\delta_{ik}\tau_{jl} + \delta_{jk}\tau_{il} + \delta_{il}\tau_{jk} + \delta_{jl}\tau_{ik} - 2\delta_{kl}\tau_{ij}). \tag{6}$$

From this definition, we can see that $\mathbf{B}$ does not possess $(ij) \longleftrightarrow (kl)$ symmetry generally. The system may be unstable when

$$\det |\mathbf{B}| = 0 \tag{7}$$

for the first time.

The following loading modes are considered.

(i) Uniaxial deformation:

$$e_{ij} = e\delta_{i3}\delta_{j3} \qquad i, j = 1, 2, 3. \tag{8}$$

In this mode, a strain is specified, and the strain energy is evaluated by subtracting a reference energy, which is calculated using the theoretical lattice constant, on the basis of a total-energy calculation. The corresponding stretches of the three axes are $\lambda_1 = \lambda_2 = 1$, $\lambda_3 < 1$ for compression, and $\lambda_3 > 1$ for tension.

(ii) Uniaxial loading:

$$\tau_{ij} = \sigma \delta_{i3}\delta_{j3} \qquad i, j = 1, 2, 3. \tag{9}$$

For a given longitudinal strain, let the transverse lattice contract or dilate to make the total energy arriving a minimum, which corresponds to zero stress (traction) on the lateral faces. Due to the crystal symmetry, the transverse contraction or dilation is the same in the two transverse directions. With the longitudinal strain and the corresponding transverse strain, the strain energy of the uniaxial loading is calculated. The corresponding stretches of the three axes are: for compression, $\lambda_1 = \lambda_2 > 1$, and $\lambda_3 < 1$; for tension, $\lambda_1 = \lambda_2 < 1$, and $\lambda_3 > 1$.

(iii) Biaxial proportional extension:

$$
\begin{aligned}
e_{22} &= \alpha e_{33} \neq 0 \\
e_{ij} &= 0 \qquad \text{otherwise.}
\end{aligned}
\tag{10}
$$

The *ab initio* pseudopotential plane-wave method is implemented. On the basis of the mechanism of Hamman [28] and Troullier and Martins [29], soft first-principles pseudopotentials are generated using the package DgncppB [25, 26]. The package Fhi96md [27], which employs a first-principles pseudopotential and a plane-wave basis set, is used to perform the DFT total-energy calculation. In our calculations, the local density approximation (LDA) with the exchange and correlation energy functional developed by Perdew and Zunger [30] is adopted.

Two supercells are designed in our calculations: one is a four-atom supercell, for use in considering the equilibrium properties and elastic constants, uniaxial deformation and loading along [001], and biaxial deformation along [010] and [001]; the other one is a three-atom supercell for use in considering uniaxial deformation and loading along [111]. Due to the calculation of the stress and elastic constants, the precision must be evaluated carefully. $E_{cut} = 12$ Ryd is sufficient in our pseudopotential plane-wave calculations. Due to the discontinuous nature of the occupation number of metal electrons, a large number of k-space samples must be used to reach sufficient precision. A smear parameter Δ is introduced to decrease the number of k-points. Our calculation shows that $\Delta = 0.058$ Ryd already gives a satisfactory result. The corresponding k-meshes are $8 \times 8 \times 8$ for the four-atom supercell, and $10 \times 10 \times 6$ for the three-atom supercell.

Table 1. Elastic moduli of Al for the equilibrium state. The length unit is the Å, and $T = 300$ K, with the experimental lattice constant. $C_{11} + C_{12}$, $C_{11} - C_{12}$, and C_{44} are the elastic constants of single crystal; the other moduli are those for isotropic materials.

	a_0	$C_{11} + C_{12}$	$C_{11} - C_{12}$	C_{44}	B	G	E	ν	A
Experiment ($T = 300$ K) [32]	4.05	168	46	28	76.0	26.0	70.0	0.35	1.22
Present work ($T = 0$ K)	3.97	183	61.4	37.4					
Mehl *et al* ($T = 0$ K) [34]	3.99	184	58.0	33.0					
Sun and Kaxiras ($T = 0$ K) [33]	3.95		58.8	45.5					
Present work ($T = 300$ K)	4.05	164	44.8	28.1	74.7	25.6	69.0	0.347	1.25
Mehl *et al* ($T = 300$ K) [34]	4.05	150	50	31	67.0	28.0	75.0	0.31	1.24
Sun and Kaxiras ($T = 300$ K) [33]	4.05		45	29.7					

3. Equilibrium properties and elastic constants

As a test, we have calculated the equilibrium lattice constant and elastic constants of bulk Al. Face-centred cubic Al has three independent elastic constants, i.e. C_{11}, C_{12}, C_{44}. The equilibrium lattice constant a_0 and the bulk modulus B_0 are obtained by fitting the energy–volume curve to the Murnaghan equation of state [31]. The relation between the bulk modulus B_0 and the elastic constant is $B_0 = (C_{11} + 2C_{12})/3$. From the uniaxial deformation along the [001] direction and the trigonal strain along the [111] direction, C_{11} and C_{44} are obtained. The results are given in table 1.

The theoretical lattice constant, $a_0 = 3.97$ Å, is 2% smaller than the experimental value, $a_0 = 4.05$ Å, and the corresponding elastic constants are 10% larger than the experimental values [32] measured at room temperature. This difference is typical of DFT-LDA calculations, and can be seen clearly from other first-principles results. Sun and Kaxiras [33] pointed out that the elastic constants are sensitive to the lattice constant of the crystal, and calculated the corresponding data using the lattice constants at room temperature. On the basis of the linear augmented-plane-wave (LAPW) method, Mehl *et al* [34] made similar calculations, and gave the bulk modulus, Young's modulus, shear modulus, average Poisson ratio, and anisotropy of isotropic materials with an orientation average. We also calculated the elastic moduli using the experimental lattice constants, and we present the results in table 1. All of the theoretical calculations are in good agreement with experimental data, and better results are given by our calculation. However, it is worth noting that we performed our calculations of the strength and stability using the theoretical lattice constant. Any externally imposed strain and stress should be excluded to get accurate results.
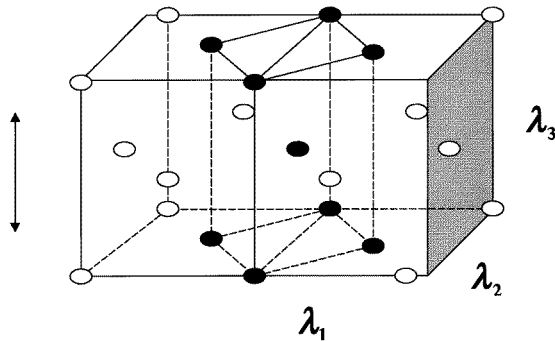

Figure 1. Two fundamental cells of the face-centred tetragonal lattice and body-centred tetragonal lattice within the same lattice.

4. [001] uniaxial loading and [001] uniaxial deformation

A four-atom face-centred tetragonal supercell was designed for investigating [001] uniaxial loading and [001] uniaxial deformation. [100], [010], and [001] were selected as the X-, Y-, and Z-axes. In the initial equilibrium state, the f.c.t. structure is f.c.c. With the same f.c.t. cell, the b.c.t. cell can be obtained by a rotation $\pi/4$ along [001]. This relation can be found from figure 1. We start from the unstressed f.c.c. state where $\lambda_1 = \lambda_2 = \lambda_3 = 1$, and let the Z-axis be compressed: on the prescribed path, the lattice must pass through the state

$\lambda_3 = \lambda_1/\sqrt{2} = \lambda_2/\sqrt{2}$ where the b.c.t. structure becomes a b.c.c. one. The cubic symmetry at this point implies that the loads are hydrostatic. For [001] uniaxial loading, since the transverse loads are always zero, the axial load in this state should be zero. Since the load must be tensile as $\lambda_3 \to \infty$ and compressive as $\lambda_3 \to 0$, the existence of two unstressed states on the primary path of [001] loading implies a third zero point in general. Obviously, the third one does not have any symmetry higher than tetragonal. The state located at the central unstressed point is always unstable for its local energy maximum. For a detailed analysis and proof of the general forms of the energy versus stretch and stress versus stretch
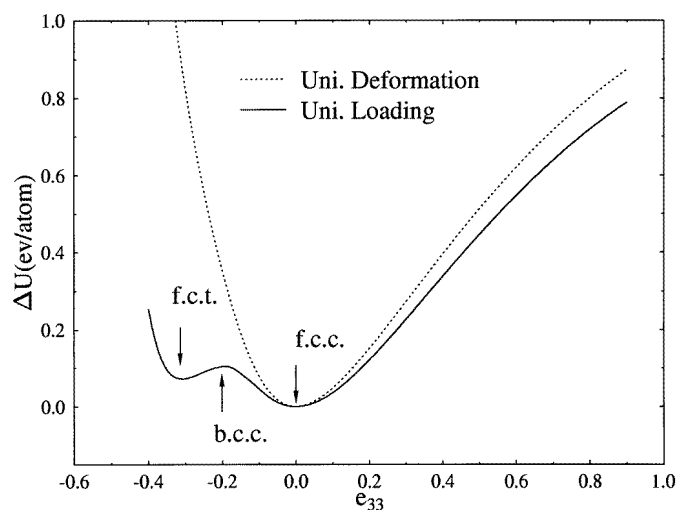
(a)
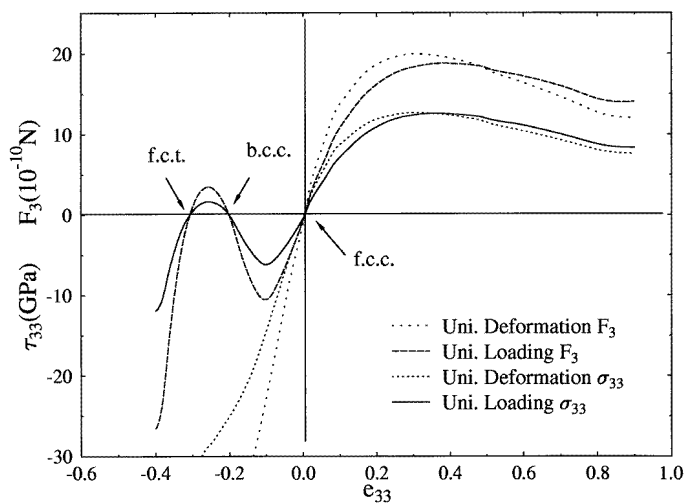
(b)

Figure 2. The calculated strain energy (a), and force and stress (b) during [001] deformation and [001] loading for the theoretical lattice constant.

relationships, the reader is referred to the original paper by Milstein [35, 36].

For tetragonal symmetry of the crystal under uniaxial loading and uniaxial deformation along the [001] direction, the number of independent elastic constants is reduced to six: C_{33}, C_{12}, $C_{13} = C_{23}$, $C_{11} = C_{22}$, $C_{44} = C_{55}$, and C_{66}; all of the other C_{ij} are equal to zero. Since we are more interested in uniaxial loading, we analyse its stability. Using equations (6), (7), and (9), we write the instability criteria for [001] uniaxial loading as follows:

$$(C_{33} + \sigma)(C_{11} + C_{12}) - 2C_{13}(C_{13} - \sigma) \leqslant 0 \tag{11}$$

$$C_{11} - C_{12} \leqslant 0 \tag{12}$$

$$C_{44} + \frac{1}{2}\sigma \leqslant 0 \tag{13}$$

$$C_{66} \leqslant 0. \tag{14}$$

The first expression involves the vanishing of the bulk modulus, and is referred to as the spinodal instability criteria. The second instability involves symmetry breaking (bifurcation) with volume conservation; it may be identified as tetragonal shear breaking, and is referred to as the Born instability. In this case, the crystal can branch away from the tetragonal path to a face-centred orthorhombic path under uniaxial dead loading; that is, the branching is $\delta\lambda_1 = -\delta\lambda_2 \neq 0$ with $\delta\lambda_3 = 0$ and $\delta\tau_{11} = \delta\tau_{22} = \delta\tau_{33} = 0$. The condition $C_{66} = 0$, when the C_{ij} are reckoned relative to the f.c.t. crystal axes, is equivalent to $C_{11} - C_{12} = 0$ when the C_{ij} are computed relative to the axes of the b.c.t. cell. So, for the state where $C_{66} = 0$ (referred to the f.c.t. axes), the tetragonal crystal branches to a body-centred orthorhombic path under uniaxial loading. $C_{44} + \frac{1}{2}\sigma = 0$ gives another shear instability.

Energy versus strain and stress, and force versus strain curves are given in figure 2 (unless otherwise stated, the strain, force, and stress given in the figures are the physical strain, applied force, and Cauchy stress). There exists only one energy minimum under uniaxial deformation. Any departure from the minimum for this loading mode leads to a rapid increase of the strain energy. Due to the triaxial stresses for the uniaxial deformation, its strain energy is always greater than the uniaxial loading. This is the same with Milstein's conclusion: the uniaxial loading represents the lowest-energy path between any two Bain paths. However, additional local maximum and local minimum states are found under uniaxial compression. The longitudinal and transverse strain at the local maximum are $e_{33} = -0.20$ and $e_{11} = 0.1313$ respectively; the ratio of the stretching, $(1 - 0.2)/(1 + 0.1313) = 0.7071$, is approximately equal to $1/\sqrt{2}$. The corresponding structure is b.c.c. with the lattice constant 3.176 Å, as expected. The remaining local minimum state is a f.c.t. structure with $e_{33} = -0.305$. From figure 2(b), we see that all three extremes are stress-free. Because the b.c.c. structure is located at a local maximum, it is unstable.

The elastic constants and corresponding stability range under [001] uniaxial loading are shown in figure 3. C_{66} is always negative over the range $[-0.40, -0.128]$, which includes the unstressed f.c.t. state. This means that, although the stress-free f.c.t. structure is at the local minimum of the uniaxial loading, it is still unstable against shear loading. Based on the explanation of C_{66}, we see that this f.c.t. state can transform to a body-centred orthorhombic state under uniaxial compression. The range of the spinodal instability under compression is $[-0.263, -0.119]$. The b.c.c. state lies at a double instability.

From figure 2(b), the compressive strength of the [001] uniaxial loading is -5.62 GPa with $e_{33} = -0.1$. During tension, the stress approaches its maximum of 12.54 GPa with $e_{33} = 0.36$. However, $C_{11} - C_{12}$ and $C_{44} + \frac{1}{2}\sigma$ have already become negative when e_{33} exceeded 0.272, and the corresponding stress is 12.1 GPa. This gives the lower limit of the tensile strength. Two possible branchings are triggered at this critical strain. With
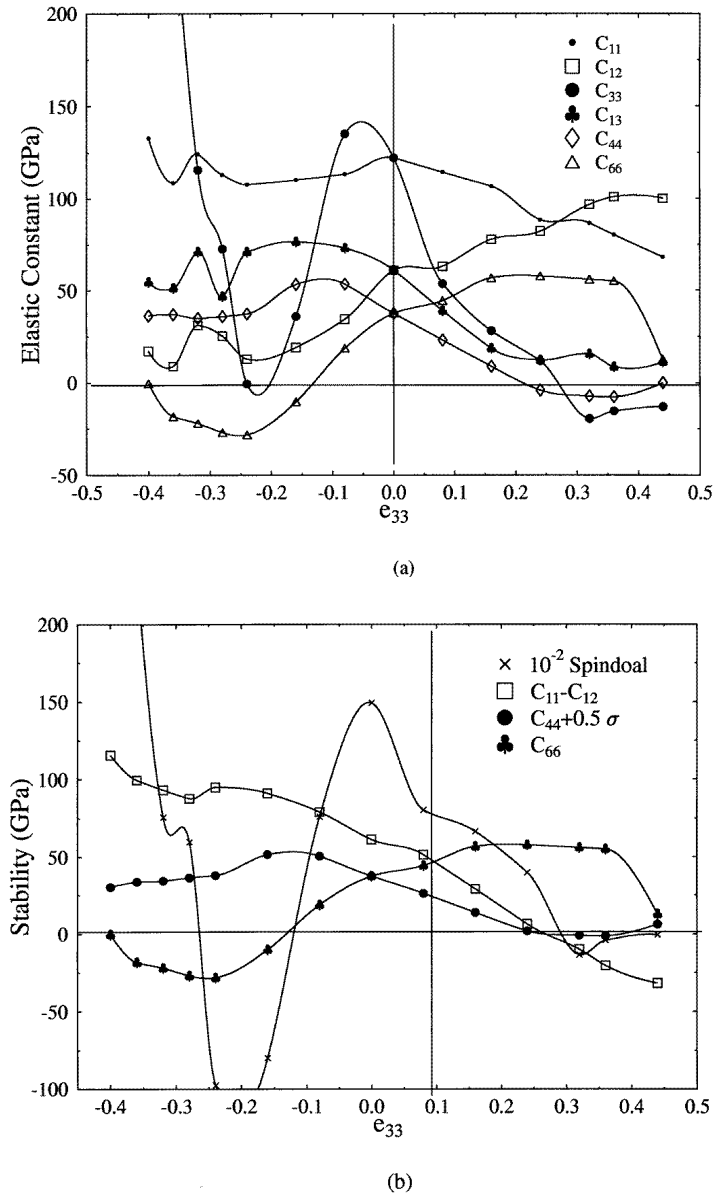
(a)

(b)

Figure 3. The calculated elastic constants (a) and stability (b) under [001] loading for the theoretical lattice constant.

$C_{11} - C_{12} = 0$, the tetragonal lattice will transform via a face-centred orthorhombic path and finally become a stable b.c.c. state [37]. With $C_{44} + \frac{1}{2}\sigma = 0$, the orthorhombic symmetry will be lost. However, which branching takes place depends on the higher-order elastic modulus. By means of pseudopotential methods based on a proposed model potential, Senoo *et al* [16] obtained a compressive strength of approximately -5.0 GPa, with a strain of -0.11, and the unstressed b.c.c. structure occurred at a strain of -0.2. These results are very similar to ours. However, the tensile strength which they obtained,

17.4 GPa with a strain of 0.42, is greater than ours. The $C_{11} - C_{12} = 0$ branching was assumed to take place at a strain of 0.15 in their work. Paxton *et al* [18] calculated the ideal-twin stress of Al on the basis of the FP-LMTO method. The corresponding value, $0.14 \frac{1}{3}(C_{11} - C_{12} + C_{44}) = 4.61$ GPa (here the C_{ij} are the elastic constants of the theoretical lattice), is approximately one third of our tensile strength.
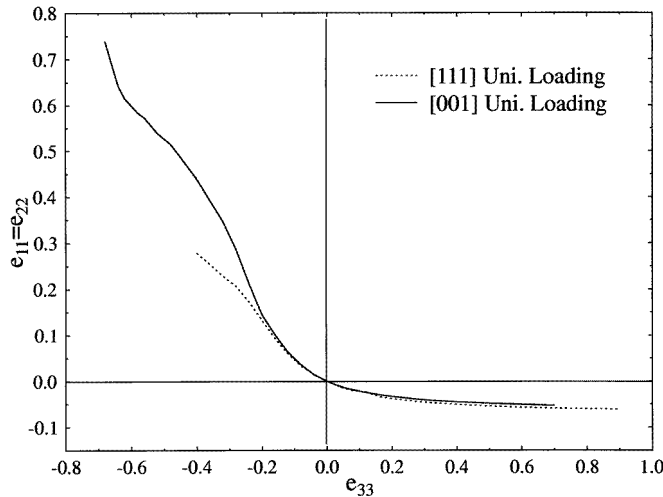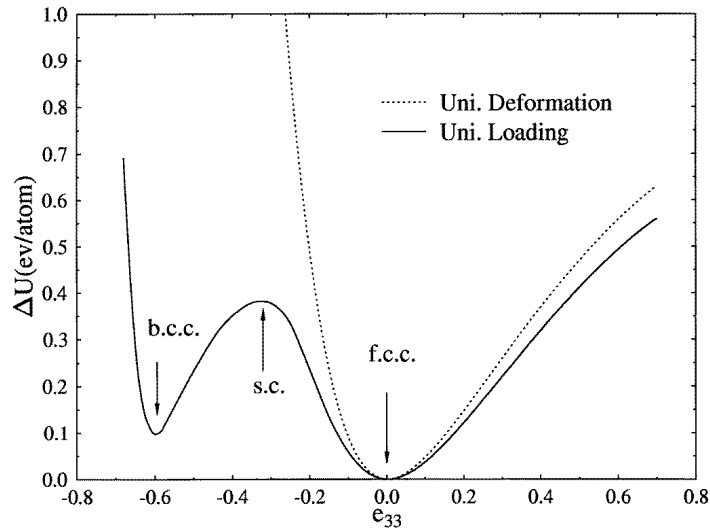

Figure 4. The calculated transverse strain for [001] loading and [111] loading with the theoretical lattice constant.

Unlike the findings for Ni [10–12], Cu [8], and α-Fe [9] obtained by Milstein *et al*, the uniaxial stress and force for Al are always lower than for uniaxial deformation before they approach the maximum. The transverse strain versus longitudinal strain is given in figure 4, and the corresponding Poisson ratio is positive along the whole path of uniaxial loading.
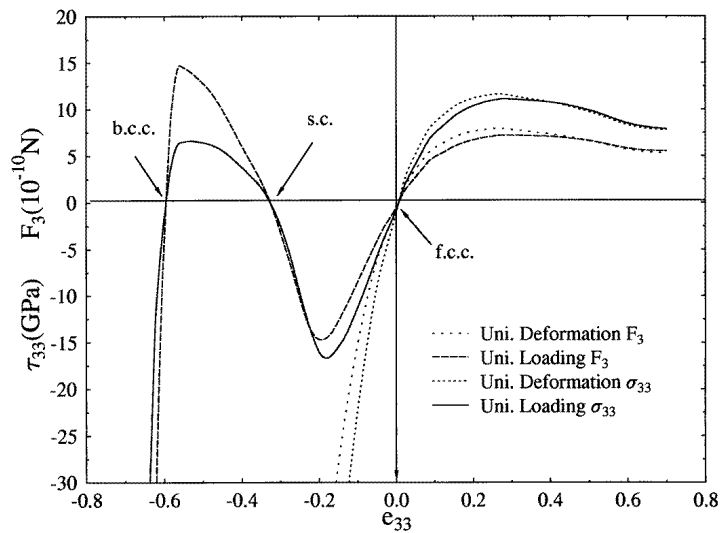
5. [111] uniaxial loading and [111] uniaxial deformation

For the case of [111] uniaxial loading and [111] uniaxial deformation, the supercell is designed as follows: the planar vectors are identical to primitive f.c.c. lattice vectors, for instance along [110] and [101] directions; the third lattice vector is in the [111] direction; and here we select three layers. In each layer, there is only one atom.

The path of deformation considered is axisymmetric, and all directions transverse to [111] are equally stretched or fixed. The axisymmetric path of deformation under [111] loading and [111] deformation consequently passes through three cubic configurations: f.c.c., s.c., and b.c.c. with increase of the compression. To illustrate this, a single quantity, r, the ratio of the longitudinal to the transverse stretch under loading, is defined. Three smallest tetrahedra are cut separately from f.c.c., s.c., and b.c.c. structures, as shown in figure 5. The bottom plane ABC is just the {111} plane, and the direction of OD is [111]. The ratios of the heights and edge lengths of the bottom plane are $\sqrt{6}/3$, $\sqrt{6}/6$, $\sqrt{6}/12$, i.e. 1, 0.5, 0.25. These ratios are just values of r, which we defined above. When r decreases from 1 to 0.25 during compression, the cubic f.c.c., s.c., and b.c.c. structures appear sequentially. The details can be found from figure 5. During [111] uniaxial loading, the transverse load is always zero, and cubic symmetry requires the three cubic configurations to be stress-free. However, during [111] uniaxial deformation, there is always a transverse load, and cubic

D

F. C. C.

$AC = BC = AB = 2^{1/2}/2$

$DA = DB = DC = 2^{1/2}/2$

$DO/AB = 6^{1/2}/3$

A

C

O

B

D

S. C.

$AC = BC = AB = 2^{1/2}$

$DA = DB = DC = 1$

$DO/AB = 6^{1/2}/6$

A

C

O

B

D

B. C. C.

$AC = BC = AB = 2^{1/2}$

$DA = DB = DC = 3^{1/2}/2$

$DO/AB = 6^{1/2}/12$

A

C

O

B

Figure 5. The three smallest tetrahedra cut separately from f.c.c., s.c., and b.c.c. structures. The length unit of each tetrahedron is the lattice constant of the corresponding original lattice. The bottom plane is just the {111} plane, and the triangle ABC is an equilateral triangle; the direction of OD is [111]. The ratio of OD to CB is the ratio of the longitudinal stretch to the transverse stretch.

symmetry of b.c.c. and s.c. indicates hydrostatic compression. For the transverse contraction under [111] loading, the s.c. and b.c.c. states will occur earlier than the [111] deformation.

The calculated results are given in figure 6. Just like in the [001] case, there exists only one minimum under uniaxial deformation, and the strain energy is always higher than the uniaxial loading. Under uniaxial loading, another local maximum and local minimum are obtained; the form of the energy versus stretch relation is just same as for [001] loading. From figure 4, we get $e_{33} = -0.333$ at the local maximum point with $e_{11} = -0.334$; the corresponding r, 0.5, is simply that for the unstressed s.c. configuration. This state is unstable for the local energy maximum. At the local minimum, $e_{33} = -0.59$ and $e_{11} = 0.64$; the corresponding r, 0.25, is that for unstressed b.c.c. structure. From a simple geometric calculation, we obtain the lattice constants of stress-free s.c. and b.c.c. structures: 2.648 Å and 3.253 Å respectively. The corresponding elastic constants are: (s.c.) $C_{11} + C_{12} = -10.1$ GPa, $C_{11} - C_{12} = -24.9$ GPa, and $C_{44} = 4.4$ GPa; (b.c.c.) $C_{11} + C_{12} = 65.19$ GPa, $C_{11} - C_{12} = -48.92$ GPa, and $C_{44} = 26.7$ GPa. From these values, we see that both s.c. and b.c.c. structures are unstable—even the b.c.c. structure located at the local minimum of the uniaxial loading. A shear instability always

(a)

(b)

Figure 6. The calculated strain energy (a), and force and stress (b) for [111] deformation and [111] loading with the theoretical lattice constant.

accompanies the unstressed s.c. and b.c.c. states. On the basis of the present and previous discussions, we conclude that for f.c.c. Al, a stable b.c.c. structure cannot be obtained by uniaxial compression along any equivalent [001] and [111] directions. The possible Bain transformation from stable f.c.c. to stable b.c.c. structure is branching caused by uniaxial tension.

Because of the lower symmetry under [111] loading and the numerical nature of the first-principles calculations, the analysis of the stability for this loading mode is difficult,

Table 2. The strength of Al calculated for different loading modes; here, TS means tensile strength, and CS means compressive strength.

	Uniaxial deformation (GPa)	$\epsilon_{33}\epsilon_{11} = \epsilon_{22}$	Uniaxial loading (GPa)	$\epsilon_{33}\epsilon_{11} = \epsilon_{22}$
[001] TS	12.65	0.30, 0.0	12.1	0.272, −0.0386
[001] CS			−5.62	−0.1, 0.049
[111] TS	11.52	0.265, 0.0	11.05	0.295, −0.0453
[111] CS			−15.89	−0.177, 0.110
Shear strength [18]	4.61			

and is hence omitted except for several special cases, i.e. the initial f.c.c., and unstressed s.c. and b.c.c. states. From figure 6(b), we can see that the stress and force for the uniaxial loading are always smaller than the uniaxial deformation. The maximum of the tensile stress is 11.05 GPa at $e_{33} = 0.295$, and the maximum magnitude of the compressive stress is 15.89 GPa at $e_{33} = -0.177$. The tensile strength and critical strain are similar to those for [001] tension; however, the compressive strength and critical strain are significantly greater than those for the [001] uniaxial compression. (The details are given in table 2.) This can be attributed to the symmetry of the materials. Under uniaxial compression, the stable f.c.c. crystal in the [001] case approaches other extreme structures more quickly than in the [111] case. This point is obvious from the following comparison. Under [001] loading, the stress-free b.c.c. and f.c.t. structures are approached at $e_{33} = -0.2$ and $e_{33} = -0.305$, where the f.c.t. structure represents the local minimum and the initial f.c.c. structure represents the overall minimum. The energy barrier obtained from these minima is as follows:

$$\Delta E_{\text{f.c.c.}\rightarrow\text{f.c.t.}} = 0.1047 \text{ eV/atom} \qquad \Delta E_{\text{f.c.t.}\rightarrow\text{f.c.c.}} = 0.0319 \text{ eV/atom}.$$

For the [111] loading, the strains of the unstressed s.c. and b.c.c. configurations are -0.333 and -0.59, where the b.c.c. structure represents the local minimum. The corresponding energy barrier is as follows:

$$\Delta E_{\text{f.c.c.}\rightarrow\text{b.c.c.}} = 0.3766 \text{ eV/atom} \qquad \Delta E_{\text{b.c.c.}\rightarrow\text{f.c.c.}} = 0.2766 \text{ eV/atom}.$$

A higher energy barrier and critical strain to transitions are needed for [111] compression.

6. Biaxial proportional extension

Biaxial proportional extension is considered here. In the present paper, we deal with extension along the [010] and [001] directions; volume relaxations are not considered. The strain ratios between [010] and [001] are 0.25, 0.5, 0.75, and 1. The results are given in figure 7. With increase of the ratio, the energy, stress, and maximum stress increase. This is because more energy is needed with a higher transverse strain for the same longitudinal strain. However, the critical strains are similar for different proportional loading modes.

7. The *ab initio* database for aluminium

Using total-energy calculations from first principles, Robertson *et al* [22] and Payne *et al* [23] constructed an *ab initio* database for aluminium, which includes 171 structures with coordination number ranging from 0 to 12 and nearest-neighbour distance ranging from
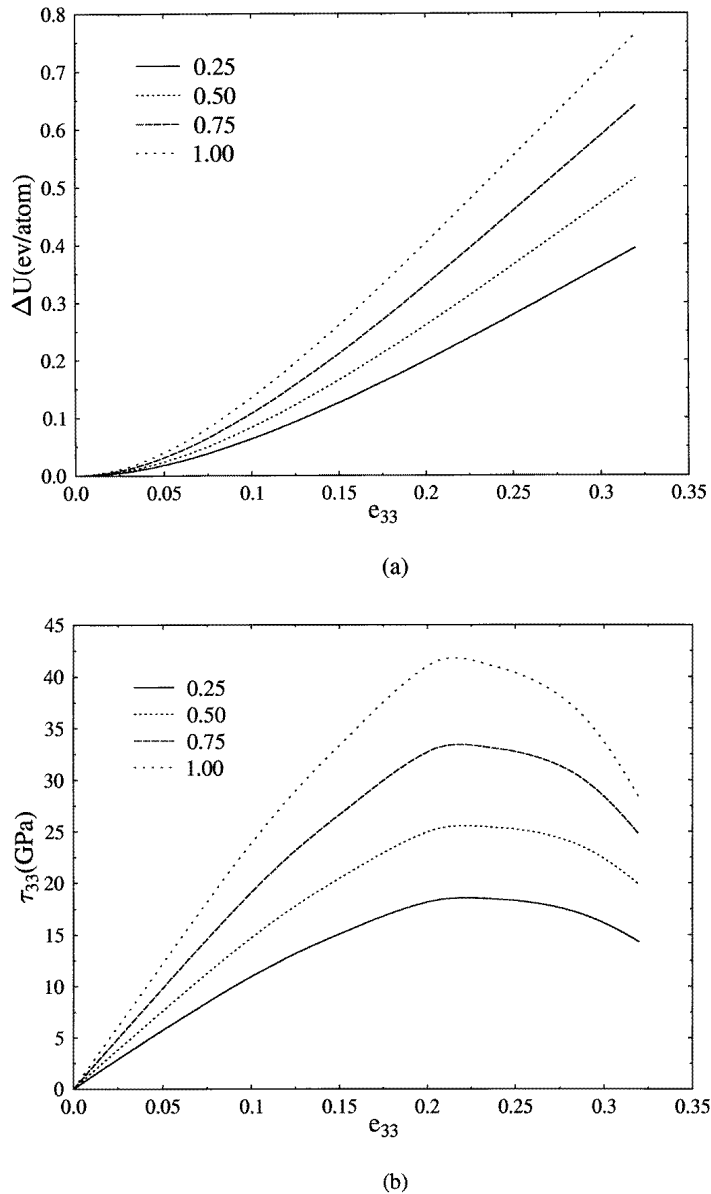
(a)

(b)

Figure 7. The calculated strain energy (a) and stress (b) during biaxial proportional extension, with the difference ratios along the [010] and [001] directions, for the theoretical lattice constant.
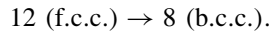
2.0 Å to 5.7 Å, for fitting and testing interatomic potentials. The energies (per atom) of all of the structures are listed with the corresponding nearest-neighbour distances. The 18 basic structures were calculated self-consistently, and the remaining 153 structures, obtained using non-self-consistent calculations, were generated from the hydrostatic pressure. However, the force, range of stability, and branching points, which are important for determining the topologies of the energy surfaces, were not given in [22] and [23].

In our investigations, all of the total-energy calculations are self-consistent; the basic

structures are four-atom and three-atom f.c.c. supercells; three loading modes (i.e. uniaxial deformation, uniaxial loading, and biaxial proportional extension) and two loading directions (i.e. [001] and [111]) are considered. The uniaxial loading path connects structures with different coordination numbers; for example, for the [111] case, from right to left,

$$12 \text{ (f.c.c.)} \rightarrow 6 \text{ (s.c.)} \rightarrow 8 \text{ (b.c.c.)}$$
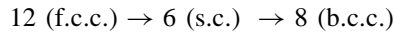
and for the [001] case,

$$12 \text{ (f.c.c.)} \rightarrow 8 \text{ (b.c.c.)}.$$

The complete energy and force–stress curves are plotted. In particular, the ranges of stability and branching points for [001] uniaxial loading are presented. The stabilities of three extreme points of [111] uniaxial loading are also given. This information is essential to the determination of the functional form of the interatomic potential.

8. Summary and conclusions

On the basis of DFT total-energy calculations and stability theory given by Hill and Milstein [2, 3, 7] and Wang *et al* [13, 14], we have given a detailed investigation of the mechanical response of f.c.c. aluminium for different loading modes and loading directions. We reached the following conclusions.

(1) In view of the requirements of crystal symmetry, the general forms of the energy versus stretch, and stress versus stretch relations for uniaxial loading of cubic crystal can be described as follows: one local minimum, one local maximum, and one overall minimum for the energy versus stretch curve, which are related to three unstressed states. The state in the middle is always unstable because of its positioning at an energy maximum.

However, when we consider a more complicated crystal, for example one with diamond structure, or alloys [38, 39], the conclusions above should be treated with caution. In such cases, the symmetry is determined by both the structural parameters and the atomic ordering, and some symmetry-dictated extrema may be lost.

(2) The complete stress–strain curves for uniaxial deformation and uniaxial loading along the [001] and [111] directions, and for biaxial proportional extension are obtained. The magnitudes of the stress and force for the uniaxial deformation are always greater than those for the uniaxial loading in the [001] and [111] directions over the range of stability. The stability range for [001] uniaxial loading is given explicitly. The tensile and compressive strengths along the [001] and [111] directions are presented.

(3) Along the path of [001] uniaxial loading, the local minimum, local maximum, and overall minimum correspond to unstressed f.c.t, b.c.c., and f.c.c. structures; under [111] uniaxial loading, they relate to stress-free b.c.c., s.c. and f.c.c. states, respectively. The intermediate states in both cases are unstable as they lie at local maxima. Although the f.c.t. state for [001] uniaxial loading and b.c.c. state for uniaxial [111] loading lie at local minima, they are still unstable against the shear instability. It is worth noting that the b.c.c. configurations for [001] and [111] loading are different configurations. Their lattice constants are 3.176 Å and 3.253 Å, and the former is located at a local maximum while the latter is located at a local minimum.

A stable b.c.c. state of Al metal cannot be obtained by uniaxial compression along any equivalent [001] and [111] direction. The possible Bain transformation is branching from the prescribed path of uniaxial tension along equivalent [001] or [110] directions.

(4) The tensile strength is similar along the [001] and [111] directions. For the higher energy barrier for [111] uniaxial compression, the compressive strength is greater than in the [001] case.

(5) The present results add to the existing *ab initio* database.

Acknowledgments

References

[1] Born M 1940 *Proc. Camb. Phil. Soc.* **36** 160
     Born M and Huang K 1956 *Dynamical Theory of Crystal Lattices* (Oxford: Clarendon)
[2] Hill R 1975 *Math. Proc. Camb. Phil. Soc.* **77** 225
[3] Hill R and Milstein F 1977 *Phys. Rev.* B **15** 3087
[4] Milstein F and Hill R 1979 *Phys. Rev. Lett.* **43** 1411
[5] Milstein F and Hill R 1977 *J. Mech. Phys. Solids* **25** 457
[6] Milstein F and Hill R 1978 *J. Mech. Phys. Solids* **26** 213
[7] Milstein F 1982 *Mechanics of Solids* ed H K Hopkins and M J Sewell (Oxford: Pergamon) p 417
[8] Milstein F and Farber B 1980 *Phil. Mag.* A **42** 19
[9] Milstein F 1971 *Phys. Rev.* B **3** 1130
[10] Milstein F 1973 *J. Appl. Phys.* **44** 3833
[11] Milstein F and Huang K 1978 *Phys. Rev.* B **18** 2529
[12] Milstein F, Hill R and Huang K 1980 *Phys. Rev.* B **21** 4282
[13] Wang J, Yip S, Phillpot S and Wolf D 1993 *Phys. Rev. Lett.* **77** 4182
[14] Wang J, Li J, Yip S, Phillpot S and Wolf D 1995 *Phys. Rev.* B **52** 12 627
[15] Zhou Z and Joós B 1996 *Phys. Rev.* B **54** 3841
[16] Senoo M, Fujishiro I and Hirano M 1984 *Bull. JMSE* **27** 2680
[17] Esposito E, Carlsson A E, Ling D D, Ehrenreich H and Gelatt C D Jr 1980 *Phil. Mag.* A **41** 251
[18] Paxton A T, Gumbsch P and Methfessel M 1991 *Phil. Mag. Lett.* **63** 267
[19] Šob M, Wang L G and Vitek V 1997 *Mater. Sci. Eng.* A **234–236** 1078
     Šandera P, Pokluda J, Wang L G and Šob M 1997 *Mater. Sci. Eng.* A **234–236** 370
[20] Milstein F, Fang H and Marschall J 1994 *Phil. Mag.* A **70** 621
[21] Fox S and Hansen H J F 1996 *Phys. Rev.* B **53** 5119
[22] Robertson I J, Thomson D, Heine V and Payne M C 1994 *J. Phys.: Condens. Matter* **6** 9963
[23] Payne M C, Robertson I J, Thomson D and Heine V 1996 *Phil. Mag.* B **73** 191
[24] Truesdell C and Toupin R 1960 *Handbuch der Physik* vol III/1, ed S Flügge (Berlin: Springer) p 226
[25] Fuchs M and Scheffler M 1998 *Comput. Phys. Commun.* at press
[26] Gonze X, Stumpf R and Scheffler M 1991 *Phys. Rev.* B **44** 8503
[27] Bockstedte M, Kley A, Neugebauer J and Scheffler M 1997 *Comput. Phys. Commun.* **107** 187
[28] Hamman D R 1989 *Phys. Rev.* B **40** 2980
[29] Troullier N and Martins J L 1991 *Phys. Rev.* B **43** 1993
[30] Perdew J and Zunger A 1981 *Phys. Rev.* B **23** 5048
[31] Murnaghan F D 1944 *Proc. Natl Acad. Sci. USA* **50** 697
[32] Simmons G and Wang H 1971 *Single Crystal Elastic Constants and Calculated Aggregated Properties: A Handbook* 2nd edn (Cambridge, MA: MIT Press)
[33] Sun Y and Kaxiras E 1997 *Phil. Mag.* A **75** 1117
[34] Mehl M J, Klein B M and Papaconstantopoulos D A 1994 *Principles (Intermetallic Compounds 1)* ed J H Westbrook and R L Fleischer (London: Wiley) ch 9

[35] Milstein F 1980 *J. Mater. Sci* **15** 1071
[36] Milstein F 1980 *Solid State Commun.* **34** 653
[37] Milstein F and Farber B 1980 *Phys. Rev. Lett.* **44** 277
[38] Cralevich P J, Weinert M, Sanchez J M and Watson R E 1994 *Phys. Rev. Lett.* **72** 3076
[39] Šob M, Wang L G and Vitek V 1997 *Comput. Mater. Sci.* **8** 100